Cellular Oncology 28 (2006) 127–139
IOS Press

Review

Non-invasive *in vivo* imaging in small animal research

V. Koo [a,*], P.W. Hamilton [b] and K. Williamson [a]

[a] *Uro-oncology Research Group, Queen's University Belfast, Northern Ireland, UK*
[b] *Bio-Imaging & Informatics Research Group Centre Cancer Research & Cell Biology, Queen's University Belfast, Northern Ireland, UK*

Abstract. Non-invasive real time *in vivo* molecular imaging in small animal models has become the essential bridge between *in vitro* data and their translation into clinical applications. The tremendous development and technological progress, such as tumour modelling, monitoring of tumour growth and detection of metastasis, has facilitated translational drug development. This has added to our knowledge on carcinogenesis. The modalities that are commonly used include Magnetic Resonance Imaging (MRI), Computed Tomography (CT), Positron Emission Tomography (PET), bioluminescence imaging, fluorescence imaging and multi-modality imaging systems. The ability to obtain multiple images longitudinally provides reliable information whilst reducing animal numbers. As yet there is no one modality that is ideal for all experimental studies. This review outlines the instrumentation available together with corresponding applications reported in the literature with particular emphasis on cancer research. Advantages and limitations to current imaging technology are discussed and the issues concerning small animal care during imaging are highlighted.

Keywords: Animal model, non-invasive, *in vivo*, imaging, CT, PET, MRI, bioluminescence, fluorescence

1. Introduction

In vivo molecular imaging in animals is an expanding discipline in biomedical research in the current post-genomic era. The driving force comes from the advancement in molecular and cellular techniques, the increased numbers of animal models and the development of novel imaging probes with complementary imaging systems. Non-invasive *in vivo* imaging is a major advantage over conventional cytology/histology microscopy techniques, which involve chemical fixation of removed tissues from which it can be difficult to generate quantitative data [41].

It is now possible to develop non-invasive *in vivo* imaging of specific molecular and cellular mechanisms; to simultaneously monitor multiple molecular events; to track specific molecular targets; to optimise drug and gene therapy; to visualise drug effects at the molecular and cellular level; and to assess disease progression [33]. *In vivo* imaging in animal models has facilitated the study of thresholds, complementation and redundancy within biological pathways [19] as well as the visualisation of the temporal and spatial biodistribution of the molecular probe and its related biological pathways.

Furthermore, longitudinal imaging of the same animal model using bio-imaging assays at multiple timepoints can achieve more valuable information than would be obtained from multiple individual animals. In these systems the animal acts as its own control and the dynamic data charts the progressive visual biological changes and therapeutic response without the sacrifice of a large number of experimental animals. Tumour xenografts grown subcutaneously or orthotopically in nude mice and syngeneic mice and rat models can now be used to investigate the effects of novel therapeutics. This approach has been harnessed to monitor tumour growth and metastasis in prostate [63] and breast [40]; to chart the development of lung cancer and to plot colon tumour regression following mitomycin c and 5-FU therapy [25].

*Corresponding author: Dr. Vincent Koo, Institute of Pathology, Centre Cancer Research & Cell Biology, Queen's University Belfast, Grosvenor Road, Belfast, BT12 6BL, UK. Tel.: +44 7880500453; Fax: +44 2890632736; E-mail: vkoo76@gmail.com.

Table 1
Features of the most common imaging techniques (modified from Lyons, 2005 [32])

Modality	Basis	Resolution	Acquisition time	Advantage	Disadvantage
PET	High energy γ-rays	1–2 mm	mins	High sensitivity	Cyclotron required to generate short-lived radioisotope
					Radiation to animal
SPECT	Low energy γ-rays	1–2 mm	mins	High sensitivity	Radiation to animal
					10–100$\times$ less sensitive than PET
					Relatively low resolution
MRI	Radiowaves	25 to 100 μm	mins to hours	Highest spatial resolution	Low sensitivity
					Long acquisition time
					Long image processing time
CT	X-rays + contrast	50 μm	mins	Good anatomical resolution	Relatively poor soft-tissue contrast
					Radiation to animal with CT contrast
Fluorescence imaging	Visible and near-infrared light	1 to 10 mm	secs to mins	High sensitivity	Prone to attenuation with increased tissue depth
				No radiation	Probes with emission wavelength $<$600 nm prone to autofluorescence
				Easy and quick to image	
Bioluminescence imaging	Visible light	1 to 10 mm	mins	High sensitivity	Low anatomic resolution
				No radiation	Light emission prone to attenuation with increased tissue depth
				Provides relative measure of cell viability or function	

2. Imaging techniques

There has been considerable progress in the development of non-invasive small animal *in vivo* imaging technology. Magnetic Resonance Imaging (MRI), Computed Tomography (CT), Positron Emission Tomography (PET) and optical imaging (bioluminescence and fluorescence) are the most popular techniques utilised by researchers over recent years (Table 1). As yet, no single imaging technique is ideal for all applications because specifications vary [32].

2.1. Computer Tomography (CT)

Although not strictly a 'molecular' imaging technique, CT has been developed specifically for high anatomical resolution imaging of small animals [5,39]. CT imaging relies on the principle that various tissue types differentially absorb X-rays as they pass through the body. As the relatively low X-ray photon-energy source of 25–50 keV is used, a high resolution/CCD detector system rotates around the body of the animal to capture images. A typical scan of an entire mouse at a resolution of 100 μm would take about 15 minutes. Higher spatial resolution would require a longer period of scanning.

In order for CT to have molecular imaging ability, specific CT probes (probably of iodine-based or barium-based for X-ray contrast), similar to PET, have been designed and used concurrently with CT scanning. Unfortunately the use of contrast agent produces an ionisation effect that results in radiation damage via

superoxides and free radicals. Since the sensitivity and spatial resolution is also dependent on the duration of CT exposure and amount of contrast agent used, the radiation dose from a CT ultimately limits the repeated imaging of the same animal.

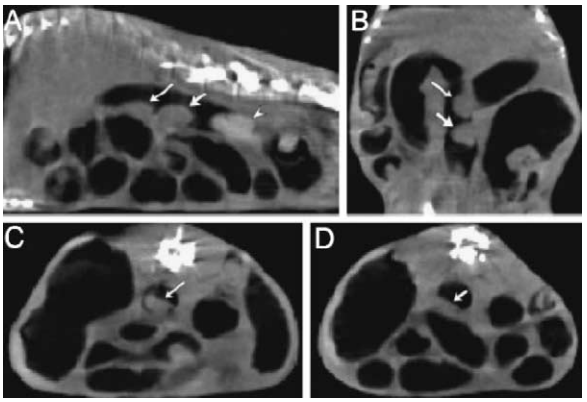

Fig. 1. Micro-CT colography prone images of an anaesthetised mouse in sagittal (A), coronal (B) and axial (C and D) positions. There are 2 colonic tumours (arrows) which were easily discriminated from luminal faecal pellet (arrow head in A) [43].

Unlike clinical CT scanners which use X-ray photon energy greater than 50 keV, animal scanners use lower energy which desirably results in up to 20× higher X-ray attenuation, thus allowing superior soft tissue discrimination in comparison to its clinical equivalent. Unfortunately, the overall poor soft tissue contrast still necessitates the use of iodinated contrast to delineate the internal organs of the animal. CT has been employed in non-invasive *in vivo* imaging to monitor colonic tumour growth (Fig. 1), to investigate bone regeneration and to detect of tumours (Table 2).

3. Positron Emission Tomography (PET) and Single Photon Emission Computed Tomography (SPECT)

PET imaging relies on probes/tracers known as isotopes that can be administered to the subjects to generate an identifiable image. The underlying principle is that PET isotopes emit $\beta+$ radiation (positrons) over

Table 2
Summary of CT application and instrumentation

Authors	Probe/contrast agent	Target tissue/cells	Animal model	Instruments and software	Application
Weber et al., 2004 [58]	ITG (1,3-bis [7-(3-amino-2,4,6-triiodophenyl) heptanoyl]-2-oleoyl-glycerol)	Liver tumours generated from injection of syngeneic CT26 cells	Murine hepatic tumour model using male BALB/c mice	MicroCT scanner (Micro-CAT I, Imtek, Knoxville, TN) Imtek software (MicroCAT Data Acquisition v3.0, Imtek, Inc.) for reconstruction of image Amira software (Amira Advanced Visualization, Data Analysis, and Geometry Reconstruction v2.3, San Diego, CA)	Monitoring of liver tumour dimensions
Gauthier et al., 2005 [20]	–	Bone	Model of bone regeneration in female New Zealand White rabbits (3–3.5 kg)	MicroCT (μCT 20, Scanco Medical AG, Bassersdorf, Switzerland)	Monitoring of new bone formation
Pickhadt et al., 2004 [43]	–	Colorectal murine tumour	C57BL/6J mice	MicroCT scanner (Micro-CAT I, Imtek, Knoxville, TN)	Detection of colonic polyp in 3D
Brown et al., 2005 [9]	–	Hyaloid vasculature of the eye	CD-1 mice	MicroCT MS-8 scanner (Enhanced Vision Systems, Inc, London, Ontario, Canada)	Characterization of hyaloid vascular structure of the eyes
Thrailkill et al., 2005 [54]	–	Bone	Female non-obese diabetic mice	MicroCT-40 (Scanco, Bassersdorff, Switzerland) and the manufacturer's software	Measurement of *de novo* bone formation during tibial distraction osteogenesis

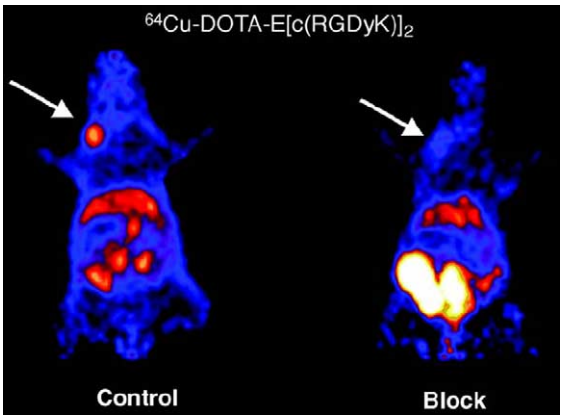

Fig. 2. MicroPET images of MDA-MB-435 breast tumour bearing athymic nude mice 2 h after administration of 400 μCi of ^{64}Cu-DOTA-E[c(RGDyK)]$_2$, with (left) and without (right) a co-injected blocking dose of c(RGDyK), a known $\alpha_v\beta_3$ integrin antagonist. The ability to inhibit tumour uptake with a blocking dose of c(RGDyK) demonstrates receptor-specific tumour activity accumulation of this tracer. Reprinted from *Molecular Imaging and Biology*, **6**(5), 350–359, Chen X., Liu S., Hou Y. et al., MicroPET imaging of breast cancer $\alpha_v\beta_3$-integrin expression with ^{64}Cu-labelled dimeric RGD peptides. Copyright 2004, with permission from Elsevier [12].

time. Each positron undergoes an annihilation reaction with an electron which results in the generation of two 511 keV photons (γ-rays) that are detected. The high energy γ-rays generated are detected and converted into visible light, which in turn is detected by light sensors and image processing units [68].

PET isotopes have different half-times ($T_{1/2}$) which range from minutes to days e.g. oxygen (^{15}O, $T_{1/2}$ = 2 min); nitrogen (^{13}N, $T_{1/2}$ = 10 min); carbon (^{11}C, $T_{1/2}$ = 20 min); fluorine (^{18}F, $T_{1/2}$ = 110 min), copper (^{64}Cu, $T_{1/2}$ = 12 h) and iodine (^{124}I, $T_{1/2}$ = 4 days). This facilitates the distinction between tracers whose function is based on biochemical processes that take place on different time-scales.

A well-known example of an isotope, 18-fluorodeoxyglucose (^{18}FDG), is widely applied in tumour studies. It accumulates in tumour specific sites on the basis that tumour cells have a greater glucose uptake rate and glycolytic metabolism than normal tissues [21]. Many other radiopharmaceuticals can be engineered, most commonly from "biologic" positron emitters such as ^{18}F and ^{11}C, to target specific molecular targets within defined *in vivo* biochemical pathways and processes [11]. Because the amounts of isotope probes required are in nanomolar concentrations or less and therefore very low, certain biological processes can be imaged without disturbing the biological process. Another advantage is that repeated imaging can be carried out on the same animal pre- and post-introduction of isotope probes, thereby allowing the animal to act as its own control.

SPECT is a distinct form of radionuclide imaging that differs from PET in that isotopes are direct gamma emitters in single direction. This necessitates different instrumentation for detection and this results in a limitation to the detection efficiency (to around 10^{-4} of number of γ-rays) of SPECT. Typically used isotopes include 123-iodine (^{123}I) and 99m-technetium (^{99m}Tc).

Applications of PET have included the imaging of xenograft models of brain, breast and ovarian tumours through exploitation of the arginine–glycine–aspartate (RGD) motif interaction with integrin receptor sites. RGD-labelled with $\alpha_v\beta_3$ integrin antagonist tracer have been used to demonstrate imaging of receptor-specific accumulation in mouse breast tumour model shown in Fig. 2. PET has also been employed to visualise endothelial receptors (Table 3).

In the past, PET was only used for larger animals, but with the incorporation of better technology and improved imaging resolution, small animal imaging is now possible. The major limitations of PET are its spatial resolution and image noise. Spatial resolution of PET scans is typically about 2^3 mm^3 [13]. Newer generation scanners can achieve a resolution of about 1^3 mm^3 [10] and have a relatively high sensitivity approximately 10^{-11} to 10^{-12} mole/l.

3.1. Magnetic Resonance Imaging (MRI)

MRI uses a large magnet to generate a magnetic field around the subject. The magnetic field causes hydrogen atoms to align themselves in water and organic compounds, creating what is known as a magnetic dipole. The specific radiofrequency (RF) coils inside the bore of the magnet generate a temporary RF pulse, capable of changing the alignment of these dipoles. Once the pulse ceases, the dipoles return or 'relax' to their normal baseline alignment. The relaxation behaviour of the dipoles is described by both T1 and T2 relaxation. Both parameters are different for different tissues resulting in contrast in MRI imaging. Depending on the timing of sequence the contrast can be predominantly T1- or T2-weighted.

Modified techniques of MRI extend the capability to obtain further functional information and will probably be available for small animal imaging in the future. Diffusion-weighted imaging uses the changes

Table 3
Summary of PET and SPECT application and instrumentation

Authors	Probe/contrast agent	Target tissue/cells	Animal model	Instruments and software	Application
Wu et al., 2005 [64]	^{64}Cu-radiolabeled tetrameric RGD	UG87MG brain glioma	Xenograft model in female athymic nude mice	MicroPET R4 scanner (Concorde Microsystems Inc, USA)	Target $\alpha_v\beta_3$ integrin in tumour cells
Johnström et al., 2005 [26]	^{18}F-endothelin-1	Endothelin receptors in rat lung, liver and kidney	Male Sprague-Dawley rat	MicroPET P4 scanner (Concorde Microsystems, Knoxville, USA)	Visualise endothelin receptors in various organs
Olafsen et al., 2005 [38]	^{111}In-DOTA 10H8 minibody and antibody, ^{111}In-MX-DTPA trastuzumab	Breast tumour MCF7/HER2	Xenograft model in female nude mice	MicroPET P4 scanner (Concorde Microsystems, Knoxville, USA)	Antibody-based targeted delivery of radioisotopes to tumour cells
Chen et al., 2004 [12]	^{64}Cu-radiolabeled dimeric RGD	MDA-MB-435 breast carcinoma	Xenograft model in female athymic nude mice	MicroPET R4 scanner (Concorde Microsystems, Knoxville, TN)	Target $\alpha_v\beta_3$ integrin in tumour cells
Janssen et al., 2002 [24]	^{111}In- and ^{99m}Tc-radiolabeled dimeric RGD peptides ^{90}Y RGD peptide	NIH:OVCAR-3 ovarian carcinoma	Xenograft model in female nude BALB/c mice	SPECT: Single head gamma camera, parallel hole medium energy collimator (Siemens Orbiter, Siemens, Inc., Hoffman Estate, IL)	Target $\alpha_v\beta_3$ integrin in tumour cells

RGD – small peptides containing the Arg–Gly–Asp amino acid sequence.

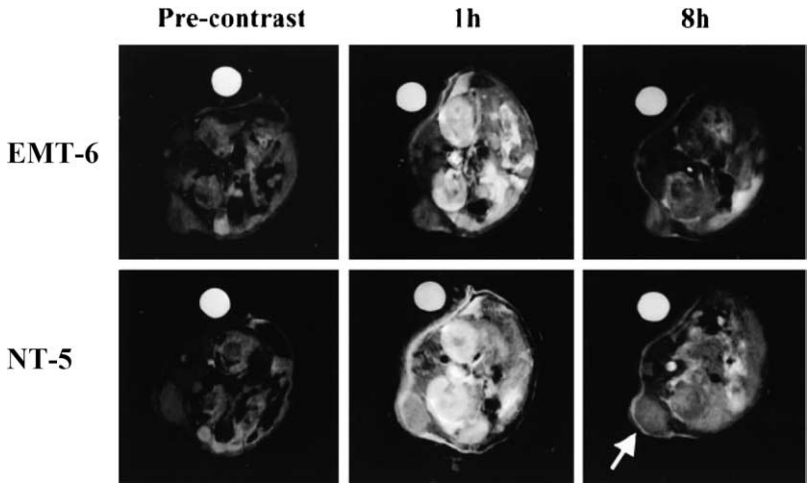

Fig. 3. MR T1-weighted images of control EMT-6 (which do not express HER-2/*neu*) and NT-5 tumours (labelled with a biotinylated monoclonal antibody to HER-2/neu) obtained before administration of the contrast agent (avidin-GdDTPA conjugate) and at 1 h, 8 h after contrast. *Arrows* show enhanced signal from the tumour at the 8 h time point for the HER-2/*neu* expressing NT-5 tumour [1].

in mobility of water molecules to obtain information on microscopic tissue characteristics [21]. Perfusion-weighted imaging exploits reporter probes for monitoring haemodynamic status. Magnetic resonance spectroscopy utilises the differential imaging spectra obtained from the molecular composition of the tissue being investigated. MRI has been applied in imaging of xenograft animal tumour models for detection of HER-2/*neu* receptors (Fig. 3), the characterisation of tumour neovascularisation [45] and monitoring T-cell recruitment [29]. Kircher exploited the use of additional chemicals in tandem with magnetic contrast agents when he used highly derivatised cross linked iron oxide (CLIO-HD) to highlight T-lymphocytes in

Table 4
Summary of Magnetic Resonance Imaging application and instrumentation

Authors	Probe/contrast agent	Target tissue/cells	Animal model	Instruments and software	Application
Bos et al., 2004 [7]	SPIO	Rat mesenchymal stem cell (MSC)	Lewis 1A rats	1.5-T clinical unit (Gyroscan Intera; Philips, Best, the Netherlands) Imaging software (IDL; RSI, Boulder, CO)	Tracking intravascularly administered SPIO-labeled MSCs in kidney and liver
Preda et al., 2004 [45]	B22956/1 Protein binding contrast agent	MDA-MB-435 breast tumour	Orthotopic xenograft model in female athymic rats	2 T Bruker Omega CSI-II (Bruker Instruments, Fremont, CA) Sun SPARC 10 workstation Image processor (Sun Microsystems, Mountain View, CA). Image analysis programme (MRVision Co., Menlo Park, CA)	(1) Detection of tumour microvessels (2) Monitoring of antiangiogenic therapy
Artemov et al. 2003 [1]	Gadolinium labelled avidin	Pre-labeled biotin HER-2/*neu* receptor in NT-5 mouse mammary tumour	Female HER-2/*neu* transgenic mice	4.7 T animal scanner (Omega; GE/Bruker)	Detection of HER-2/*neu* receptor
Winter et al., 2003 [63]	Paramagnetic nanoparticle	Vx-2 Rabbit tumour	New Zealand white rabbit	1.5 T scanner (NT Intera with Master Gradients, Philips Medical Systems, Best, Netherlands) EasyVisions v5.1, Philips Medical Systems, BEST, Netherlands. MATLAB (The MathWorks, Inc., Matick, MA)	Detection of early tumour angiogenesis by targeting $\alpha_v\beta_3$ integrin
Beckmann et al., 2003 [4]	SPIO	Rat macrophages	Xenograft model of kidney transplantation in Lewis rats	4.7 T Biospec 47/40 spectrometer (Bruker, Karlsruhe, Germany)	Assessment of perfusion of transplanted kidney
Kircher et al., 2003 [29]	CD8+ T lymphocytes labeled with CLIO-HD	B16-OVA melanoma cell line	Xenograft model in female C57Bl/6 mice	8.5T scanner (Bruker DRX 360) CMIR-Image (Interactive Data Language, Research Systems Inc., Boulder, CO)	Monitoring T-cell recruitment in tumour

T – tesla (unit of magnetic flux density), CLIO-HD – highly derivatised crosslinked iron oxide, SPIO – super paramagnetic iron oxide.

his xenograft model [29]. Similarly super paramagnetic iron oxide (SPIO) has been used as a molecular probe to track mesenchymal and macrophage cells and hence generate a more informative image (Table 4).

Recently, developments in animal MRI have focussed on the development of new contrast agents that increase sensitivity and specificity. Contrast agents can be classified as non-specific, targeted and smart probes [8]. Non-specific probes such as gadolinium chelates show a non-specifically distributed pattern, and are used to measure tissue perfusion and vascular permeability. Targeted probes such as gadolinium labelled avidin and annexin V-supramagnetic iron oxide nanoparticles are designed to specifically bind to ligands such as peptides and antibodies. In one study, avidin conjugated gadolinium targeted the biotinylated Her2/*neu* receptor (Fig. 3, Table 4). Similarly, annexin V-supramagnetic iron oxide nanoparticles were used to detect apoptotic cells. The principle underlying the latter is that apoptotic cells expose phosphatidylserine, which has an affinity for annexin, on their outer membranes [50]. Smart probes tag a specific ligand similar to targeted agents, but differ in that the probe signal changes upon interaction with the specific ligand.

MRI has advantages in that it has a higher resolution, which falls within a micrometer range, compared to radionuclides and optical probes in millimetres. MRI is also attractive because of its low toxicity and the absence of ionising radiation. In certain applications, MRI can simultaneously extract physiological, molecular and anatomical information. However, a disadvantage of MRI is that it is less sensitive than radionuclide or optical imaging technique.

3.2. Optical imaging

This technique employs quantitative light emission i.e. photons to obtain measurements of relevant biological parameters, including proteins and nucleic acids within individual living cells. Further advancement comes through the development of new targeted bioluminescence probes, near-infrared fluorochromes and red fluorescent proteins [59]. To detect low levels of light or photons, a very sensitive charge coupled device (CCD) detector is used [23]. The CCD detector is silicon-based and is capable of detecting light from the visible and to the near-infrared range (NIR). This imaging modality produces excellent data from organs and structures close to the skin surface in small animals but, difficulties are encountered in deeper organs, due to light absorption in tissues and the ability to detect low photon emission through tissues. There are two main forms of optical imaging, namely fluorescence imaging (FLI) and bioluminescence (BLI).

3.2.1. Fluorescence imaging

Visible light (395 to 600 nm) is used to excite fluorescence within the subject and a camera or fluorescent microscopy system detects the emitted light from the region of interest within the subject. The commonly used strategy is to fluorescently tag the cells, tissue or molecules under investigation with substances known to fluoresce. In the recent past, a popular choice has been the green fluorescent protein (GFP) which is derived from jellyfish *Aequorea victoria.* The wild-type GFP emits light at 509 nm, while its variant EGFP has a longer emitting wavelength and is 35-fold brighter [27]. Another currently popular fluorescent protein is the red fluorescence protein (RFP), DsRed. DsRed2 is a faster maturing, more soluble variant of reef coral protein from the *Discosoma* species which allows more rapid appearance of red fluorescence together with a reduced tendency for aggregation. It has a tetrameric structure and a maximum excitation wavelength of 563 nm and maximum emission wavelength of 582 nm. Newer fluorescent probes developed from a genetic modification of RFP such as mBanana, tdTomato, mTangerine, mStrawberry and mCherry with longer emission wavelength and greater stability are now available [52].

A distinctive advantage over BLI is that FLI does not require administration of a substrate for visualisation. This overcomes the potential problem of difficult intravenous access in small animals. Fluorochromes that emit light of wavelengths greater than 600 nm should be used so that the absorbance by surrounding tissue is minimised and to ensure that background and auto-fluorescence can be distinguished [56]. Hence, using NIR fluorochromes maximises tissue penetration and minimises autofluorescence [60]. This is attributable to the lower absorption coefficients of water and haemoglobin, which are the major absorbers in tissues, at the NIR spectrum. Several applications have exploited the NIR range [31], e.g. Cy5.5 has been used to image EGF in breast tumours [28]. In addition, Quantum Dots (QD) which are nano-sized molecular probes that have long-term stability and fluoresce brightly up to NIR spectrum upon excitation, have been developed for imaging [2]. Yang et al. [66] has successfully employed DsRed2 shown in Fig. 4, which has a higher emission wavelength, to map tumour growth and metastases.

A further development to fluorescence imaging is Fluorescence Molecular Tomography (FMT). FMT employs a continuous pulse light from different sources to excite the fluorochrome label and multiple detectors arranged spatially analogous to the set up in CT or MR scanners [36,37]. Computation generates a three-dimensional image. The resulting images have a resolution of 1–2 mm, and the fluorochrome detection threshold is in the nanomolar range.

3.2.2. Bioluminescence imaging

The main difference between BLI and FLI is that light emission in BLI does not require excitation of the reporter. Light emission originates from an exergonic catalysis reaction of the substrate which releases photons of visible light [62]. One common approach used in animal models is transfection of one of the luciferase family of photo-proteins, that can be isolated either from the sea-pansy (*Renilla reniformis*) or from the North American firefly (*Photimus pyralis*), into the tumour cells prior to their inoculation into animals. Further the expression of luciferase can be controlled so that it is expressed only when required or so that it is only expressed when a gene of interest is being transcribed. The luciferase protein can catalyse

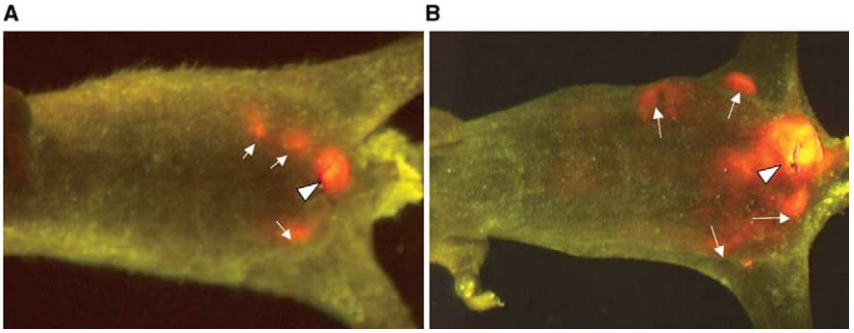

Fig. 4. (A) Whole-body fluorescence imaging of 2 weeks post-surgical implanted orthotopic PC3-DsRed primary prostate tumour (arrowhead) and metastasis in nude mice (arrows). (B) Image of the same animal 4 weeks later showing progressive tumour growth (arrow head) and extension of metastases (arrows) [66].

Table 5
Summary of Fluorescence Imaging application and instrumentation

Authors	Probe/ contrast agent	Target tissue/cells	Animal model	Instruments and software	Application
Yang et al., 2005 [66]	DsRed2	PC-3 human prostate	Male nude mice	Leica LZ12, 50W mercury lamp CCD camera (C5810, Hamamatsu Photonics) Image Pro Plus v4.0 (Media Cybernetics, SilverSpring, MD)	Monitoring of tumour growth
Yang et al., 2003 [65]	DsRed2	RFP expressing B16F0 melanoma, MMT060562 mammary, Dunning and PC-3 prostate and HCT-116 colon tumours	Nude C57/B6-GFP mice with subcutaneous melanoma/orthotopic breast/orthotopic prostate/orthotopic colon tumours	Leica LZ12, 50W mercury lamp CCD camera (C5810, Hamamatsu Photonics) Image Pro Plus 3.1 (Media Cybernetics)	Monitoring of tumour growth and metastatic progression
Ke et al., 2003 [28]	Cy5.5	Human mammary MDA-MB-468 (EGFr+) and MDA-MB-435 (EGFr−) cancer cells	Female athymic nude mice	Image intensifier (model FS9910C; ITT Night Vision, Roanoke, VA) CCD camera (CH350, Photometrics, Tucson, AZ) V++ software (Digital Optics, Auckland) and Matlab software	Monitoring of EGFR targeted therapy
Schmitt et al., 2002 [51]	GFP	Lymphoma cells	Lymphoma model in transgenic mice	Leica LZ12, 50 W mercury lamp CCD camera (C5810, Hamamatsu Photonics) Image Pro Plus 3.1 (Media Cybernetics)	Monitoring of the effects of genotype on therapeutic efficacy
Peyruchaud et al., 2001 [40]	GFP	MDA-MB-231 human breast carcinoma	Xenograft breast cancer and metastases model in female nude Balb/c mice	Fluorescence scanning system (Fluorimager; Molecular Dynamics, Sunnyvale, CA, USA)	Detection of bone metastasis

RFP – Red fluorescent protein.

luciferin (Firefly luciferase) and coelenterazine (Renilla luciferase) following their delivery to the animal, usually through tail vein injection just prior to BLI (Fig. 5). Cells expressing luciferase can be easily identified through their emission of light in the range from 400 to 620 nm [22]. The use of BLI in dynamic *in vivo* imaging was validated in a neutropenic mouse model in which antimicrobial treatment applications were monitored. This technology has become a very valuable tool which has been employed to dynamically monitor tumour growth or transcriptional activity in living animals as shown in Table 6.

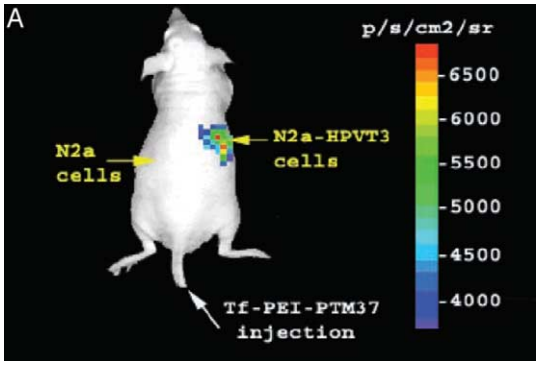

Fig. 5. Bioluminescent imaging following subcutaneous implantation with *Renilla* luciferase (N2a LucHPVT3) transfected cells (right side) or mock N2a transfected cells (left side) in a nude mouse. The tumour site expressing luciferase emitted a bioluminescent signal which was amplified through administration of *SMaRT probe (Tf-PEI-PTM37) 24 h prior to injection with the substrate coelenterazine [6]. Spliceosome-mediated RNA trans-splicing (SMaRT).

The main advantage of BLI over FLI is its capability to detect very low levels of light signal because there is virtually no background light noise. In FLI, the external light source required for fluorochrome excitation could also generate background autofluorescence from animal tissues (Fig. 5).

There are, however, some limitations in BLI. Firstly, light transmission efficiency is dependent on the tissue type being assessed. Highly vascular organ structures contain oxyhaemoglobin and deoxyhaemoglobin that absorb transmitted light which results in about a ten-fold reduction of the bioluminescence signal for every centimetre of tissue depth [16]. Secondly, because the catalytic reaction that generates bioluminescence is time- and enzyme-dependent, optimisation efforts are needed to determine the window period for optimum image capture. Comparatively, FLI may be more convenient and easier to capture images at multiple time-points, since the animal does not require intravenous administration of substrate.

Table 6
Summary of Bioluminescence Imaging application and instrumentation

Authors	Probe	Target tissue/cells	Animal model	Instruments and software	Application
Szentirmai et al., 2006 [53]	Firefly luciferase	U87MG human glioma	Xenograft tumour model in nude mice	In Vivo Imaging System IVIS® (Xenogen Corp, Alameda, CA), Living Image® software (Xenogen Corp, CA)	(1) Monitoring of tumour growth (2) Monitoring therapeutic response to adenoviruses encoding antiangiogenic soluble vascular endothelial growth factor
Massoud et al., 2004 [34]	Split synthetic renilla luciferase probes	293T human embryonic kidney tumour cells protein-protein interactions	Nude mice	In Vivo Imaging System IVIS® (Xenogen Corp, Alameda, CA), Living Image® software (Xenogen Corp, CA)	Screening for homodimeric protein–protein interactions
Jenkins et al., 2003 [25]	Firefly luciferase	PC-3M (prostate) A549 (lung) HT-29 (colon)	Xenograft tumour models of prostate lung and colon in male SCID mice	In Vivo Imaging System IVIS® (Xenogen Corp, Alameda, CA), Living Image® software (Xenogen Corp, CA)	(1) Monitoring of tumour growth and metastasis (2) Monitoring of therapeutic response to mitomycin c and 5FU
Pichler et al., 2003 [42]	Renilla luciferase	Human epidermoid carcinoma KB3-1 cells and colchicine-selected KB8-5-11 cells	Male nude mice	In Vivo Imaging System IVIS® (Xenogen Corp, Alameda, CA), Living Image® software (Xenogen Corp, CA)	Screening for multidrug resistance *MDR1* P-glycoprotein
Rocchetta et al., 2001 [48]	*lux*, bacterium-based bioluminescence system from *Photorhabdus luminescens*	*E. coli* EC14	Neutropenic mouse thigh model	In Vivo Imaging System IVIS® (Xenogen Corp, Alameda, CA), Living Image® software (Xenogen Corp, CA)	Monitoring of antimicrobial therapy

Table 7
Summary of the different imaging modalities and its application

Authors	Probe/contrast agent	Target	Animal model	Modality	Application
Chow et al., 2006 [14]	[18F] fluoride ion	Bone	BLK6 mouse	MicroPET and microCT	Validating multimodality imaging hardware
Rowland et al., 2005 [49]	[^{18}F]FDG (PET) gadodiamide (MRI)	EMT-6 mouse mammary carcinoma	Xenograft breast tumour in BALB/c mice	MRI and microPET	Monitoring of tumour growth
Ponomarev et al., 2004 [44]	*tk* (PET) *G*FP(Fluorescence) Luciferase (Bioluminescence)	U87 human glioma cells	Xenograft tumour model nude mice	Bioluminescence, fluorescence, microPET	Detection and monitoring of tumour growth
Moore et al., 2004 [35]	Cy5.5 (Fluorescence) CLIO (MRI) -EPPT	uMUC-1 antigen positive ZR-75-1 (breast), BT-20 (breast), HT-29 (colon), CAPAN-2 (pancreas), LS174T (colon), ChaGo-K-1 (lung)	Xenograft tumour model in nude mice	MRI and fluorescence microscopy	Detection and monitoring of tumour growth
Ray et al., 2003 [47]	*tk* (PET) renilla luciferase (Bioluminescence)	N2a neuronal tumour cell	Xenograft tumour model in male nude mice	Bioluminescence and microPET	Monitoring of tumour growth
Doubrouvin et al., 2001 [17]	*tk* (PET) GFP (Fluorescence)	U87 human glioma cells	Xenograft tumour model in nude rats	MicroPET and fluorescence	Monitoring p53 transcriptional activity in tumours

EPPT – synthetic peptide that has significant affinity for the uMUC-1-derived peptide PDTRP;
HSV1-tk – herpes simplex virus type 1 thymidine kinase;
CLIO – Cross-linked iron oxide.

3.3. Multimodality imaging

New ongoing research is now focusing on amalgamating image modalities. The combination of the various techniques offers a greater quality of information obtained. Unique opportunities to define more specifically the localisation of biological processes, to quantify biological activity and to characterise novel biomarkers are now possible. For example, the development of microPET/CT offers high anatomical resolution with functional information, resulting in a bimodal image [55,56]; and the development of Optical PET (OPET) detectors that can simultaneously capture PET and bioluminescence images [46].

Image co-registration is a term which describes the spatial combination of two images acquired by separate imaging modalities. The quantitative accuracy of the generated image is dependent on the accuracy of the image co-registration technique. This technique improves quantitative localisation of a molecular probe in a more detailed anatomical resolution [67]. Several sophisticated software techniques are available to co-register related intermodality images. In addition, hardware devices including a small animal imaging chamber designed to reproducibly mount on separate microCT and microPET scanners are now available [14]. Table 7 demonstrates several current applications of multimodal imaging including monitoring and detection of tumour growth and monitoring transcriptional activity.

4. Animal concerns in bio-imaging

One important aspect to consider in choosing and using the small animal imaging modality is the welfare of the animal. Several issues warrant consideration such as difficult vascular access to obtain blood samples, the small size of the animals, animal anaesthesia, optimal temperature control and exposure to radiation.

For most *in vivo* studies, anaesthesia is required to immobilise and to occasionally carry out invasive procedures. The anaesthesia should be easy to administer and of sufficient anaesthetic duration and depth for completion of experiments and imaging. Anaesthe-

sia has been induced and maintained effectively via subcutaneous, intramuscular, intravenous and inhalant routes. Depending on the anaesthetic protocol and duration of anaesthesia, the metabolic and physical effects can vary in different animals such as hepatic toxicity, hypercapnia, hypothermia, hypoxia and acidosis. In bio-functional imaging studies such as, distribution or metabolism of a therapy, alteration in blood flow and changes in organ function, anaesthesia can affect the cardio-respiratory and central nervous system which potentially introduces unwanted biases [30]. Preliminary pilot studies are advised to optimise anaesthetic protocols to the specific needs of the animal [15].

Because small animals tend to have a large surface area-to-body-mass ratio and rapid body metabolism, they are more prone to dehydration and heat loss. Hypothermia has been documented in rodents after brief 10–15 minute procedures [2,18]. Attempts to provide warmth or insulation and to restore hydration are imperative for wellbeing. Heating devices such as warm-water blankets, thermal heating pads, heated platform, heat lamps and warm air blowers have been used for animals. On the other hand, provision of warm fluid parenterally and humidified gasses can be carried out to prevent dehydration. Modalities such as CT and PET that use radioactive probes or involve radiation exposure to the animal should comply with the maximal radiation dosage. For example, in rats PET tracer doses ranges from 0.5 to 2.0 mCi and in mice ranges from 50–200 μCi.

5. Conclusion

The challenge remains to develop an instrument capable of imaging a small body volume in three dimensions using a low amount of molecular probe; providing spatial resolution that is sufficient to analyse meaningful anatomical and functional data; detecting and locating sensitively, specifically and accurately; and obtaining an image in a short capture time [33, 60]. Presently, most researchers employ CT imaging for bone-related studies because of its high anatomical resolution and bone image contrast. MRI is exploited for its excellent spatial resolution and good soft-tissue/organ image contrast. Bioluminescence imaging is often employed for assessing therapeutic response because of its excellent sensitivity whilst fluorescence imaging facilitates tumour growth monitoring because of its quick and convenient multiple time-point image capture. PET has high sensitivity and permits accurate quantitation of molecular target detection because γ-rays are not attenuated as they pass through tissue. SPECT, a distinct nuclear medicine modality, is cheaper than PET but has a slightly lower sensitivity. The multi-modality techniques which will simplify localisation of imaging are rapidly evolving.

The rapid development in biotechnology has resulted in sophisticated noninvasive *in vivo* imaging technologies that can be used to screen animals with distinct genotypes. These advances concomitant with innovative molecular techniques are facilitating drug target validation and evaluation of therapeutic efficacy. Inevitable exploitation and expansion in this field will test many hypotheses on the road towards our goals of greater understanding of the carcinogenic process and cancer therapeutics.

Acknowledgements

We would like to acknowledge the funding by DHSS Research and Development Office, Mason's Medical Foundation and SRIF Queens University Belfast. We also thank all the authors and publishers who have kindly contributed to the reprinting of figures used in this review article. We also thank Miss Rachel Yew for her support and help in the preparations of the images.

References

[1] D. Artemov, N. Mori, R. Ravi and Z.M. Bhujwalla, Magnetic resonance molecular imaging of the HER-2/neu receptor, *Cancer Res.* **63** (2003), 2723–2727.

[2] R.S. Balaban and V.A. Hampshire, Challenges in small animal noninvasive imaging, *ILAR J.* **42** (2001), 248–262.

[3] B. Ballou, B.C. Lagherholm, L.A. Ernst, M.P. Bruchez and A.S. Waggoner, Noninvasive imaging of quantum dots in mice, *Bioconjug. Chem.* **15** (2004), 79–86.

[4] N. Beckmann, C. Cannet, M. Fringeli-Tanner, D. Baumann, C. Pally, C. Bruns, H.G. Zerwes, E. Andriambeloson and M. Bigaud, Macrophage labeling by SPIO as an early marker of allograft chronic rejection in a rat model of kidney transplantation, *Magn. Reson. Med.* **49** (2003), 459–467.

[5] F. Berger, Y.P. Lee, A.M. Loening, A. Chatziioannou, S.J. Freedland, R. Leahy, J.R. Lieberman, A.S. Belldegrun, C.L. Sawyers and S.S. Gambhir, Whole-body skeletal imaging in mice utilizing microPET: Optimization of reproducibility and applications in animal models of bone disease, *Eur. J. Nucl. Med. Mol. Imaging* **29** (2002), 1225–1236.

[6] S. Bhaumik, Z. Walls, M. Puttaraju, L.G. Mitchell and S.S. Gambhir, Molecular imaging of gene expression in living subjects by spliceosome-mediated RNA trans-splicing, *Proc. Natl. Acad. Sci. USA* **101** (2004), 8693–8698.

[7] C. Bos, Y. Delmas, A. Desmouliere, A. Solanilla, O. Hauger, C. Grosset, I. Dubus, Z. Ivanovic, J. Rosenbaum, P. Charbord, C. Combe, J.W. Bulte, C.T. Moonen, J. Ripoche and N. Grenier, *In vivo* MR imaging of intravascularly injected magnetically labeled mesenchymal stem cells in rat kidney and liver, *Radiology* **233** (2004), 781–789.

[8] C. Bremer, V. Ntziachristos and R. Weissleder, Optical-based molecular imaging: contrast agents and potential medical applications, *Eur. Radiol.* **13** (2003), 231–243.

[9] A.S. Brown, L. Leamen, V. Cucevic and F.S. Foster, Quantitation of hemodynamic function during developmental vascular regression in the mouse eye, *Invest. Ophthalmol. Vis. Sci.* **46** (2005), 2231–2237.

[10] A. Chatziioannou, Y.C. Tai, N. Doshi and S.R. Cherry, Detector development for microPET II: a 1 microl resolution PET scanner for small animal imaging, *Phys. Med. Biol.* **46** (2001), 2899–2910.

[11] A.F. Chatziioannou, Molecular imaging of small animals with dedicated PET tomographs, *Eur. J. Nucl. Med.* **29** (2002), 98–114.

[12] X. Chen, S. Liu, Y. Hou, M. Tohme, R. Park, J.R. Bading and P.S. Conti, MicroPET imaging of breast cancer α_v-integrin expression with ^{64}Cu-labelled dimeric RGD peptides, *Mol. Imaging Biol*. **6** (2004), 350–359.

[13] S.R. Cherry and S.S. Gambhir, Use of positron emission tomography in animal research, *Ilar. J.* **42** (2001), 219–232.

[14] P.L. Chow, D.B. Stout, E. Komisopoulou and A.F. Chatziioannou, A method of image registration for small animal, multimodality imaging, *Phys. Med. Biol.* **51** (2006), 379–390.

[15] L.A. Colby and B.J. Morenko, Clinical considerations in rodent bioimaging, *Comp. Med*. **54** (2004), 623–630.

[16] C.H. Contag, P.R. Contag, J.I. Mullins, S.D. Spilman, D.K. Stevenson and D.A. Benaron, Photonic detection of bacterial pathogens in living host, *Mol. Mircobiol.* **18** (1995) 593–603.

[17] M. Doubrovin, V. Ponomarev, T. Beresten, J. Balatoni, W. Bornmann, R. Finn, J. Humm, S. Larson, M. Sadelain, R. Blasberg and J. Gelovani Tjuvajev, Imaging transcriptional regulation of p53-dependent genes with positron emission tomography *in vivo*, *Proc. Natl. Acad. Sci. USA* **98** (2001), 9300–9305.

[18] P.A. Flecknell, Anaesthesia of animals for biomedical research, *Br. J. Anaesth*. **71** (1993), 885–894.

[19] Gassmann, M. and T. Hennet, From genetically altered mice to integrative physiology, *News Physiol. Sci.* **13** (1998), 53–57.

[20] O. Gauthier, R. Muller, D. von Stechow, B. Lamy, P. Weiss, J.M. Bouler, E. Aguado and G. Daculsi, *In vivo* bone regeneration with injectable calcium phosphate biomaterial: a three-dimensional micro-computed tomographic, biomechanical and SEM study, *Biomaterials* **27** (2005), 5444–5453.

[21] J.L. Griffin and J.P. Shockcor, Metabolic profiles of cancer cells, *Nat. Rev. Cancer*. **4** (2004), 551–561.

[22] J.W. Hastings, Chemistries and colors of bioluminescent reactions: a review, *Gene* **173** (1996), 5–11.

[23] A. Honigman, E. Zeira, P. Ohana, R. Abramovitz, E. Tavor, I. Bar, Y. Zilberman, R. Rabinovsky, D. Gazit, A. Joseph, A. Panet, E. Shai, A. Palmon, M. Laster and E. Galun, Imaging transgene expression in live animals, *Mol. Ther.* **4** (2001), 239–249.

[24] M.L. Janssen, W.J. Oyen, I. Dijkgraaf, L.F. Massuger, C. Frielink, D.S. Edwards, M. Rajopadhye, H. Boonstra, F.H. Corstens and O.C. Boerman, Tumor targeting with radiolabeled $\alpha_v\beta_3$ integrin binding peptides in a nude mouse model, *Cancer Res.* 62 (2002), 6146–6151.

[25] D.E. Jenkins, Y. Oei, Y.S. Hornig, S.F. Yu, J. Dusich, T. Purchio and P.R. Contag, Bioluminescent imaging (BLI) to improve and refine traditional murine models of tumor growth and metastasis, *Clin. Exp. Metastasis* **20** (2003), 733–744.

[26] P. Johnström, T.D. Fryer, H.K. Richards, N.G. Harris, O. Barret, J.C. Clark, J.D. Pickard and A.P. Davenport, Positron emission tomography using 18F-labelled endothelin-1 reveals prevention of binding to cardiac receptors owing to tissue-specific clearance by ET B receptors *in vivo*, *Br. J. Pharmacol.* **144** (2005), 115–122.

[27] K. Kaneko, M. Yano, T. Yamano, T. Tsujinaka, H. Miki, Y. Akiyama, M. Taniguchi, Y. Fujiwara, Y. Doki, M. Inoue et al., Detection of peritoneal micrometastases of gastric carcinoma with green fluorescent protein and carcinoembryonic antigen promoter, *Cancer Res.* **61** (2001), 5570–5574.

[28] S. Ke, X. Wen, M. Gurfinkel, C. Charnsangavej, S. Wallace, E.M. Sevick-Muraca et al., Near-infrared optical imaging of epidermal growth factor receptor in breast cancer xenografts, *Cancer Res.* **63** (2003), 7870–7875.

[29] M.F. Kircher, J.R. Allport, E.E. Graves, V. Love, L. Josephson, A.H. Lichtman and R. Weissleder, *In vivo* high resolution three-dimensional imaging of antigen-specific cytotoxic T-lymphocyte trafficking to tumors, *Cancer Res.* **63** (2003), 6838–6846.

[30] J.C. LaManna and S.I. Harik, Regional studies of blood–brain barrier transport of glucose and leucine in awake and anesthetized rats, *J. Cereb. Blood Flow Metab.* **6** (1986), 717–723.

[31] Y. Lin, R. Weissleder and C.H. Tung, Novel near-infrared-cyanine fluorochromes: Synthesis, properties, and bioconjugation, *Bioconjug. Chem.* **13** (2002), 605–610.

[32] S.K. Lyons, Advances in imaging mouse tumour models *in vivo*, *J. Pathol.* **205** (2005), 194–205.

[33] T.F. Massoud and S.S. Gambhir, Molecular imaging in living subjects: seeing fundamental biological processes in a new light, *Genes Dev*. **17** (2003), 545–580.

[34] T.F. Massoud, R. Paulmurugan and S.S. Gambhir, Molecular imaging of homodimeric protein–protein interactions in living subjects, *FASEB J.* **18** (2004), 1105–1107.

[35] A. Moore, Z. Medarova, A. Potthast and G. Dai, *In vivo* targeting of underglycosylated MUC-1 tumor antigen using a multimodal imaging probe, *Cancer Res.* **64** (2004), 1821–1827.

[36] V. Ntziachristos and R. Weissleder, Charge-coupled-device based scanner for tomography of fluorescent near-infrared probes in turbid media, *Med. Phys.* **29** (2002), 803–809.

[37] V. Ntziachristos, C.H. Tung, C. Bremer and R. Weissleder, Fluorescence molecular tomography resolves protease activity *in vivo*, *Nat. Med.* **8** (2002), 757–760.

[38] T. Olafsen, V.E. Kenanova, G. Sundaresan, A.L. Anderson, D. Crow, P.J. Yazaki, L. Li, M.F. Press, S.S. Gambhir, L.E. Williams, J.Y. Wong, A.A. Raubitschek, J.E. Shively and A.M. Wu, Optimizing radiolabelled engineered anti-p185^{HER2} antibody fragments for *in vivo* imaging, *Cancer Res.* **65** (2005), 5907–5916.

[39] M.J. Paulus, S.S. Gleason, M.E. Easterly and C.J. Foltz, A review of high-resolution X-ray computed tomography and other imaging modalities for small animal research, *Lab. Anim. (NY)* **30** (2001), 36–45.

[40] O. Peyruchaud, B. Winding, I. Pecheur, C.M. Serre, P. Delmas and P. Clezardin, Early detection of bone metastases in a murine model using fluorescent human breast cancer cells: application to the use of the bisphosphonate zoledronic acid in the treatment of osteolytic lesions, *J. Bone Miner. Res.* **16** (2001), 2027–2034.

[41] R.D. Phair and T. Misteli, Kinetic modelling approaches to *in vivo* imaging, *Nat. Rev. Mol. Cell. Biol.* **2** (2001), 898–907.

[42] A. Pichler, J.L. Prior and D. Piwnica-Worms, Imaging reversal of multidrug resistance in living mice with bioluminescence: MDR1 P-glycoprotein transports coelenterazine, *Proc. Natl. Acad. Sci. USA* **101** (2004), 1702–1707.

[43] P.J. Pickhardt, R.B. Halberg, A.J. Taylor, B.Y. Durkee, J. Fine, F.T. Lee, Jr. and J.P. Weichert, Microcomputed tomography colonography for polyp detection in an *in vivo* mouse tumor model, *Proc. Natl. Acad. Sci. USA* **102** (2005), 3419–3422.

[44] V. Ponomarev, M. Doubrovin, I. Serganova, J. Vider, A. Shavrin, T. Beresten, A. Ivanova, L. Ageyeva, V. Tourkova, J. Balatoni, W. Bornmann, R. Blasberg and J. Gelovani Tjuvajev, A novel triple-modality reporter gene for whole-body fluorescent, bioluminescent, and nuclear noninvasive imaging, *Eur. J. Nucl. Med. Mol. Imaging* **31** (2004), 740–751.

[45] A. Preda, V. Novikov, M. Moglich, K. Turetschek, D.M. Shames, R.C. Brasch, F.M. Cavagna and T.P. Roberts, MRI monitoring of Avastin antiangiogenesis therapy using B22956/1, a new blood pool contrast agent, in an experimental model of human cancer, *J. Magn. Reson. Imaging* **20** (2004), 865–873.

[46] D.L. Prout, R.W. Silverman and A. Chatziioannou, Detector concept for OPET-A combined PET and optical imaging system, *IEEE Trans. Nucl. Sci.* **51** (2004), 752–756.

[47] P. Ray, A.M. Wu and S.S. Gambhir, Optical bioluminescence and positron emission tomography imaging of a novel fusion reporter gene in tumor xenografts of living mice, *Cancer Res.* **63** (2003), 1160–1165.

[48] H.L. Rocchetta, C.J. Boylan, J.W. Foley, P.W. Iversen, D.L. LeTourneau, C.L. McMillian, P.R. Contag, D.E. Jenkins and T.R. Parr, Jr., Validation of a noninvasive, real-time imaging technology using bioluminescent Escherichia coli in the neutropenic mouse thigh model of infection, *Antimicrob. Agents Chemother.* **45** (2001), 129–137.

[49] D.J. Rowland, J.R. Garbow, R. Laforest and A.Z. Snyder, Registration of [18F]FDG microPET and small-animal MRI, *Nucl. Med. Biol.* **32** (2005), 567–572.

[50] E.A. Schellenberger, A. Bogdanov, Jr., D. Hogemann, J. Tait, R. Weissleder and L. Josephson, Annexin V-CLIO: a nanoparticle for detecting apoptosis by MRI, *Mol. Imaging* **1** (2002), 102–107.

[51] C.A. Schmitt, J.S. Fridman, M. Yang, S. Lee, E. Baranov, R.M. Hoffman and S.W. Lowe, A senescence program controlled by p53 and p16INK4a contributes to the outcome of cancer therapy, *Cell* **109** (2002), 335–346.

[52] N.C. Shaner, P.A. Steinbach and R.Y. Tsien, A guide to choosing fluorescent proteins, *Nat. Methods* **2** (2005), 905–909.

[53] O. Szentirmai, C.H. Baker, N. Lin, S. Szucs, M. Takahashi, S. Kiryu, A.L. Kung, R.C. Mulligan and B.S. Carter, Noninvasive bioluminescence imaging of luciferase expressing intracranial U87 xenografts: correlation with magnetic resonance imaging determined tumor volume and longitudinal use in assessing tumor growth and antiangiogenic treatment effect, *Neurosurgery* **58** (2006), 365–372.

[54] K.M. Thrailkill, L. Liu, E.C. Wahl, R.C. Bunn, D.S. Perrien, G.E. Cockrell, R.A. Skinner, W.R. Hogue, A.A. Carver, J.L. Fowlkes, J. Aronson and C.K. Lumpkin, Jr., Bone formation is impaired in a model of type 1 diabetes, *Diabetes* **54** (2005), 2875–2881.

[55] D.W. Townsend, A combined PET/CT scanner: The choices, *J. Nucl. Med.* **42** (2001), 533–534.

[56] D.W. Townsend and S.R. Cherry, Combining anatomy and function: The path to true image fusion, *Eur. Radiol.* **11** (2001), 1968–1974.

[57] T. Troy, D. Jekic-McMullen, L. Sambucetti and B. Rice, Quantitative comparison of the sensitivity of detection of fluorescent and bioluminescent reporters in animal models, *Mol. Imaging* **3** (2004), 9–23.

[58] S.M. Weber, K.A. Peterson, B. Durkee, C. Qi, M. Longino, T. Warner, F.T. Lee, Jr. and J.P. Weichert, Imaging of murine liver tumor using microCT with a hepatocyte-selective contrast agent: accuracy is dependent on adequate contrast enhancement, *J. Surg. Res.* **119** (2004), 41–45.

[59] R. Weissleder, A clearer vision for *in vivo* imaging, *Nat. Biotechnol.* **19** (2001), 316–317.

[60] R. Weissleder, Scaling down imaging: molecular mapping of cancer in mice, *Nat. Rev. Cancer* **2** (2002), 11–18.

[61] R. Weissleder and U. Mahmood, Molecular imaging, *Radiology* **219** (2001), 316–333.

[62] T. Wilson and J.W. Hastings, Bioluminescence, *Annu. Rev. Cell. Dev. Biol.* **14** (1998), 197–230.

[63] P.M. Winter, S.D. Caruthers, A. Kassner, T.D. Harris, L.K. Chinen, J.S. Allen, E.K. Lacy, H. Zhang, J.D. Robertson, S.A. Wickline and G.M. Lanza, Molecular imaging of angiogenesis in nascent Vx-2 rabbit tumors using a novel $\alpha_v\beta_3$-targeted nanoparticle and 1.5 tesla magnetic resonance imaging, *Cancer Res.* **63** (2003), 5838–5843.

[64] Y. Wu, X. Zhang, Z. Xiong, Z. Cheng, D.R. Fisher, S. Liu, S.S. Gambhir and X. Chen, MicroPET imaging of glioma integrin $\alpha_V\beta_3$ expression using ^{64}Cu-labeled tetrameric RGD peptide, *J. Nucl. Med.* **46** (2005), 1707–1718.

[65] M. Yang, L. Li, P. Jiang, A.R. Moossa, S. Penman and R.M. Hoffman, Dual-color fluorescence imaging distinguishes tumor cells from induced hostangiogenic vessels and stromal cells, *Proc. Natl. Acad. Sci. USA* **100** (2003), 14259–14262.

[66] M. Yang, P. Jiang, N. Yamamoto, L. Li, J. Geller, A.R. Moossa and R.M. Hoffman, Real-time whole-body imaging of an orthotopic metastatic prostate cancer model expressing red fluorescent protein, *Prostate* **62** (2005), 374–379.

[67] H. Zaidi and B. Hasegawa, Determination of the attenuation map in emission tomography, *J. Nucl. Med.* **44** (2003), 291–315.

[68] S.I. Ziegler, Instrumentation and data acquisition, in: *Diagnostic Nuclear Medicine*, C. Schiepers, ed., Springer Verlag, Berlin, 2000, pp. 221–236.